ELSEVIER

Marine Geology 164 (2000) 13–27

MARINE GEOLOGY
INTERNATIONAL JOURNAL OF MARINE GEOLOGY, GEOCHEMISTRY AND GEOPHYSICS

www.elsevier.nl/locate/margeo

Compressional velocity structure and Poisson's ratio in marine sediments with gas hydrate and free gas by inversion of reflected and refracted seismic data (South Shetland Islands, Antarctica)

U. Tinivella[a,*], F. Accaino[b]

[a]*Osservatorio Geofisico Sperimentale, P.O. Box 2011, 34016 Trieste, Italy*
[b]*DINMA, University of Trieste, Trieste, Italy*

Received 28 July 1998; accepted 5 January 1999

Abstract

A Bottom Simulating Reflector (BSR) on the South Shetland Margin (Antarctic Peninsula) was surveyed, within the Progetto Nazionale di Ricerche in Antartide (PNRA). High resolution multichannel (MCS) reflection profiles were acquired, and a three-component Ocean Bottom Seismograph (OBS) was deployed where the BSR was particularly strong.

The compressional velocity field associated to the BSR was determined by the inversion of travel times of reflected (MCS data) and refracted (OBS data) events. Information on shear wave velocities was extracted from the horizontal components of the OBS records. The analysis indicates the presence of velocity anomalies both above and below the BSR that are not related to the lithologic characteristics of the sedimentary column, but can be associated to gas hydrate and free gas presence in pore space.

Amplitude Versus Offset (AVO) analysis was performed on Common Depth Point gathers, which correspond to the OBS position. The study determined reflection coefficient trends that provided qualitative information about gas hydrate and free gas abundance.

A theoretical model for elastic porous media was applied to quantify amounts of gas hydrate and free gas. The resulting theoretical velocity curves were compared to interval velocity obtained by seismic inversion. A quantitative estimation of free gas and gas hydrates trapped in the sediment pore spaces was made by interpreting velocity anomalies with respect to reference velocity curves (normally consolidated marine terrigenous sediments).

The comparison of the results obtained by these independent methods (seismic inversion, AVO analysis, and theoretical model) gives consistent values of Poisson's ratio and gas hydrate and free gas estimation.

Keywords: Gas hydrate; Bottom simulating reflector; Ocean bottom seismograph data; Compressional velocity; Poisson's ratio; Amplitude versus offset studies

1. Introduction

Information about the velocity field is indispensable in areas where direct measurements are not available to reveal the presence of gas hydrate-bearing layers and/or free gas-bearing layers. In fact, the hydrated sediments have an anomalously high compressional (V_p) and shear (V_s) wave velocity, that can be interpreted in terms of gas hydrate concentration when a

* Corresponding author. Fax: +39-040-327307.
E-mail address: utinivella@ogs.trieste.it (U. Tinivella).

0025-3227/00/$ - see front matter
PII: S0025-3227(99)00123-1

reference curve is known (Tinivella, 1999). However, a low compressional velocity zone can indicate the presence of free gas in pore spaces. The effect of strong acoustic impedance contrast between sediments containing gas hydrates and sediments with free gas is evident in marine seismic profiles as Bottom Simulating Reflectors (BSRs, e.g. Shipley et al., 1979). In presence of gas hydrate and free gas, models indicate that shear wave velocity increases and Poisson's ratio decreases (e.g. Hyndman and Spence, 1992; Katzman et al., 1994; Minshull et al., 1994; Andreassen et al., 1997). For this reason, studies of both compressional and shear waves provide information about the presence of clathrates and free gas in the marine sediments.

We analysed the BSR identified on the South Shetland continental margin (Antarctic Peninsula). The South Shetland margin is an accretionary prism related to the former subduction of the extinct Phoenix plate beneath the continental South Shetland Island platform (see Barker, 1982; Later and Barker, 1991, for a comprehensive review). The BSR is present in the accreted and fore arc sedimentary units along the continental slope of the margin. It is a well defined, high-amplitude, reverse-polarity and nearly continuous reflector located between 500 and 900 ms below the seafloor: it crosses seismic horizons that reflect the position and the orientation of sedimentary layers. The BSR is younger than them and is superimposed on their acoustic structure (Tinivella et al., 1998a,b).

Inversion of reflected and refracted arrivals is applied to multichannel seismic (MCS) and to a three-component Ocean Bottom Seismograph (OBS) data acquired on the South Shetland margin, in order to obtain a local compressional and shear velocity field associated to the presence of gas hydrates and/or free gas in the sedimentary layers.

Amplitude Versus Offset (AVO) analysis of MCS data is also performed at OBS location to obtain Poisson's ratio in the gas hydrate-bearing sediments. Finally, a theoretical model is applied to estimate the amount of these components in the pore space from velocity fields.

2. Acquisition and processing of seismic data

About 750 km of high resolution multichannel and single channel seismic reflection data were acquired during the cruise on the Austral summer 1996/1997 across the South Shetland margin (Fig. 1). The MCS profiles were conducted using two GI-guns with a total volume of 4 l firing every 25 m. The acquisition system consisted of a 3000 m long 120-channel analogue streamer, with hydrophone group interval of 25 m. The sampling interval was 2 ms. The conventional seismic processing applied to the data included common depth point (CDP) sorting, spherical divergence amplitude correction, bandpass filter 10–220 Hz, and multiple reduction. After reconstruction of the velocity field from seismic inversion (see Section 4), we applied the pre-stack depth migration to raw field data, in order to enhance the seismic image of the structures associated with the BSR.

A three-component OBS station was also deployed along a seismic profile where the BSR signature was particularly evident (MCS line I97206; see Fig. 1). The OBS is constituted by an acquisition system (SEDIS II), and a three-component geophone floating in high-density oil is present at the bottom of the sphere. So, apart from the seabed topography, there are two horizontal components and a vertical one. Another problem concerning this type of acquisition is the coupling between the instrument and the seafloor. In order to reduce its effects, we coupled the OBS with the ballast as well as possible. The energy source was two GI-guns, with shot spacing 50 m; the frequency of sampling was 512 Hz. The shot spacing was used to avoid generation of bands of previous shot noise (water wave and other low-velocity arrivals) that interfere with wide-angle reflection and refraction at large offset. We determined the horizontal distance of the OBS from the shot points considering the picked time of the water wave in the OBS data and the related arrival time evaluated in function of the unknown OBS location. A bandpass filter 10–75 Hz was used to increase the S/N ratio.

3. Inversion of travel times

Reflection seismic profiles are useful to reconstruct the V_p field and to explore its possible lateral variation applying inversion techniques (e.g. inversion of travel times). OBS data are necessary to investigate layers that are deeper than the BSR (from refracted waves)

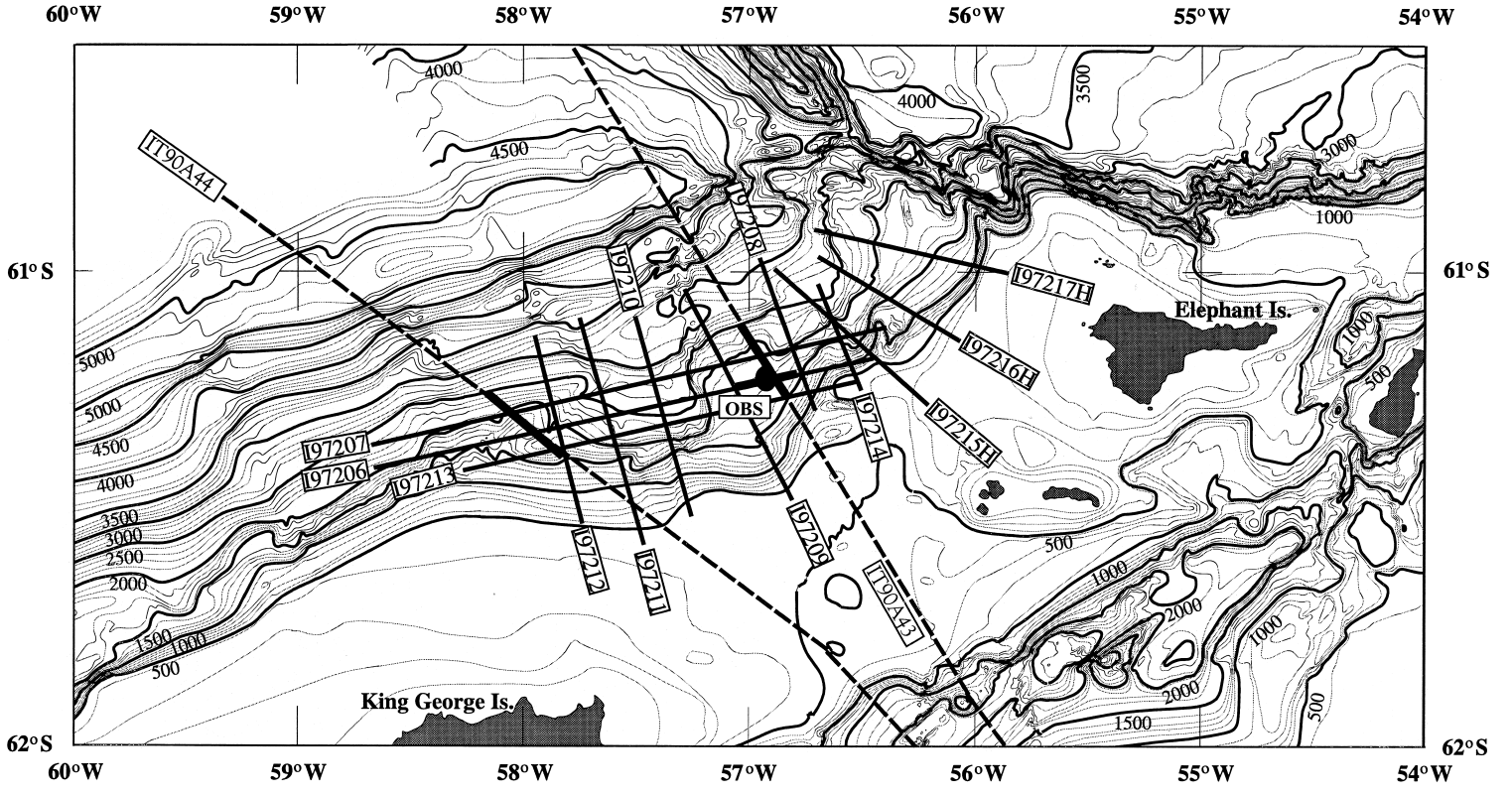

Fig. 1. Location of multichannel seismic profiles acquired on austral summer 1996/1997 (solid line) and OBS position. The dashed lines indicate the seismic lines acquired on 1989/1990. The thick solid segments indicate the parts of lines studied in this paper (Line I97206) and in the previous studies (Lines IT90A43 and IT90A44; Tinivella et al., 1998a,b). Bathymetric data after Klepeis and Lowver (1996).

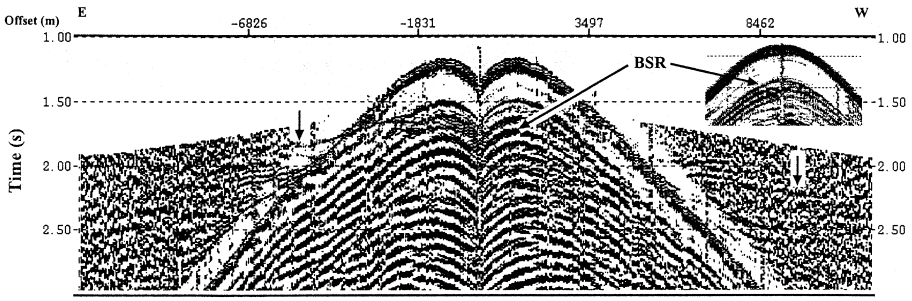

Fig. 2. Vertical component of OBS data; the time is reduced with a velocity of 3 km/s. A bandpass filter (10–75 Hz) was used to increase the S/N ratio The arrows indicate the inverted refracted events. The insert shows the BSR at not reduced time.

and to investigate the V_s structure. In fact, the deeper layers are difficult to explore using conventional reflection profiling, because a horizon that is strongly reflective, and high in the stratigraphic column (in this case the BSR) masks the underlying structure effectively (Jarchow et al., 1994). A travel time table for both MCS and OBS data was obtained by using semi-automatic picking in order to study the coherence of the signal (Tinivella, 1998). We inverted only the part of MCS line I97206 near the OBS location (see thick segment in Fig. 1).

3.1. MCS data

We identified six reflectors in the MCS data: the seafloor, the BSR, three reflectors between the two, and a more continuous reflector below the BSR. A tomographic method (Carrion et al., 1993) was used to determine the shallow compressional velocity structures by the reflected arrival in the MCS data. We inverted the arrival times of 21 contiguous hydrophone groups (seismic traces) with spacing of 25 m, providing a minimum offset of 1375 m. These traces have been selected for two reasons: (1) the trace spacing must be constant within a shot gather (it is essential in our method); and (2) the selected traces provided the optimum reflectivity and amplitude response in contiguous shot gathers.

3.2. Vertical component of OBS data

In the vertical component of the OBS data we picked the BSR, a reflector between the seafloor and the BSR (also observed in the MCS data), and refracted event (Fig. 2). The picked times were inverted following the Zelt and Smith (1992) approach, starting from the velocity model obtained by tomographic inversion of MCS data. The inversion of travel times of Zelt and Smith employs a forward ray-tracing step and damped least-squares inversion step to modify the model parameters (velocities and/or depth of layers) by minimising the difference between the observed and predicted travel times. This procedure allowed us to identify the base of the free gas layer (BGR), to obtain information about velocity field below the free gas zone, and to test the goodness of the velocity field obtained from MCS data by the tomographic inversion. The final velocity model (Fig. 3) indicates an increase of velocity in the layer above the BSR (from 2 to 2.3 km/s), that can be associated with the presence of gas hydrate in the pore spaces. Below it, a low velocity layer (1.2–1.5 km/s with a variable thickness of 100–400 m) is observed, which indicates the presence of free gas in the sedimentary sequence. The velocity in the free gas zone was confirmed by a satisfactory result of pre-stack depth migration (see Section 4). Moreover, we observed energy below the BSR in the OBS data at about 2 s at minimum offset, which could correspond with the BGR. The picking of this reflector was particularly uncertain, so that these arrivals are not considered in the inversion procedure. However, the arrival times of this energy are quite consistent with the BGR depth in the final velocity model. The compressional velocity field above the BGR is in agreement with a previous study in the area (see thick segments in Fig. 1; Tinivella et al., 1998a,b), where the tomographic analysis indicates a velocity field, from the seafloor to the BSR, increasing approximately from 1.6 to 2.3 km/s, and, from the BSR to the BGR, it shows a drop of the interval

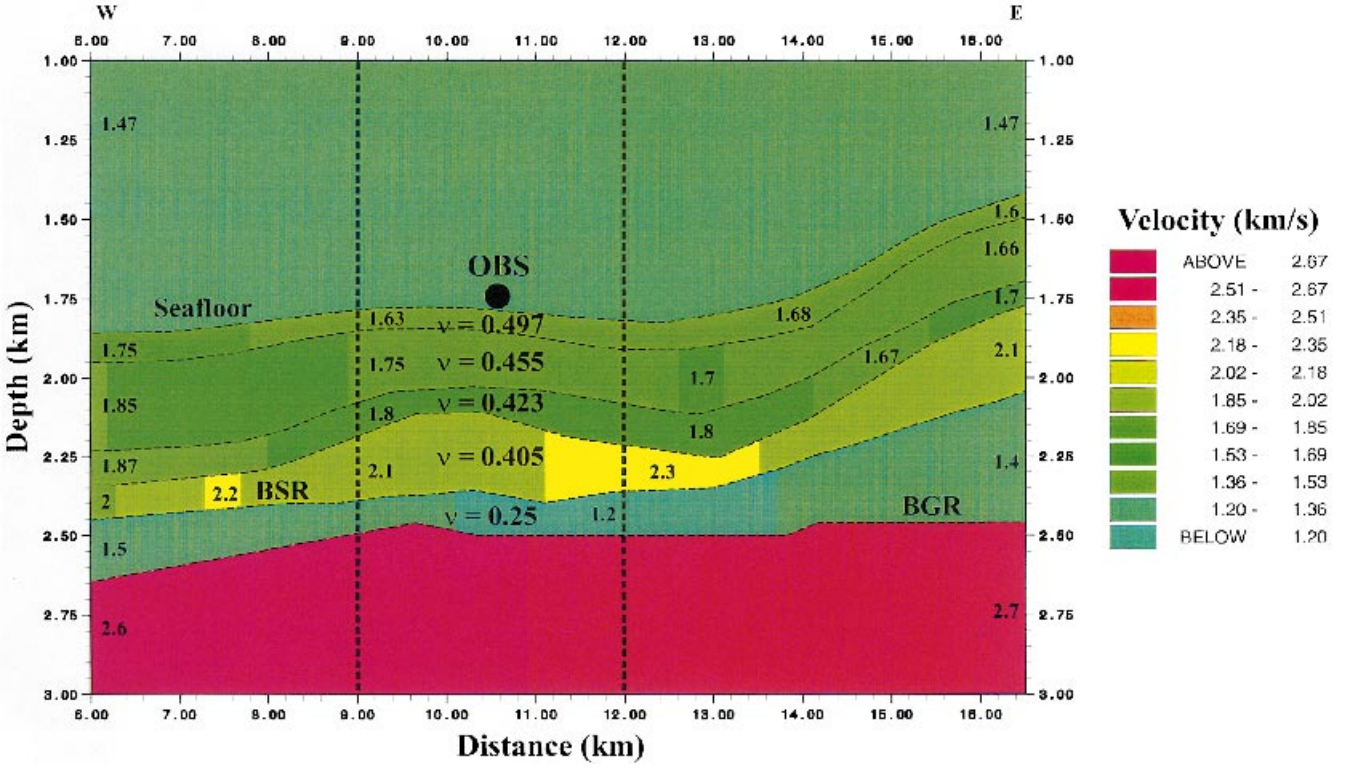

Fig. 3. Compressional velocity field after MCS and OBS data inversion. The dashed lines indicate the zone where the shear wave arrivals are inverted. Poisson's ratios, indicated as ν, are those obtained by AVO inversion above the BSR and by OBS data inversion below it (see text).

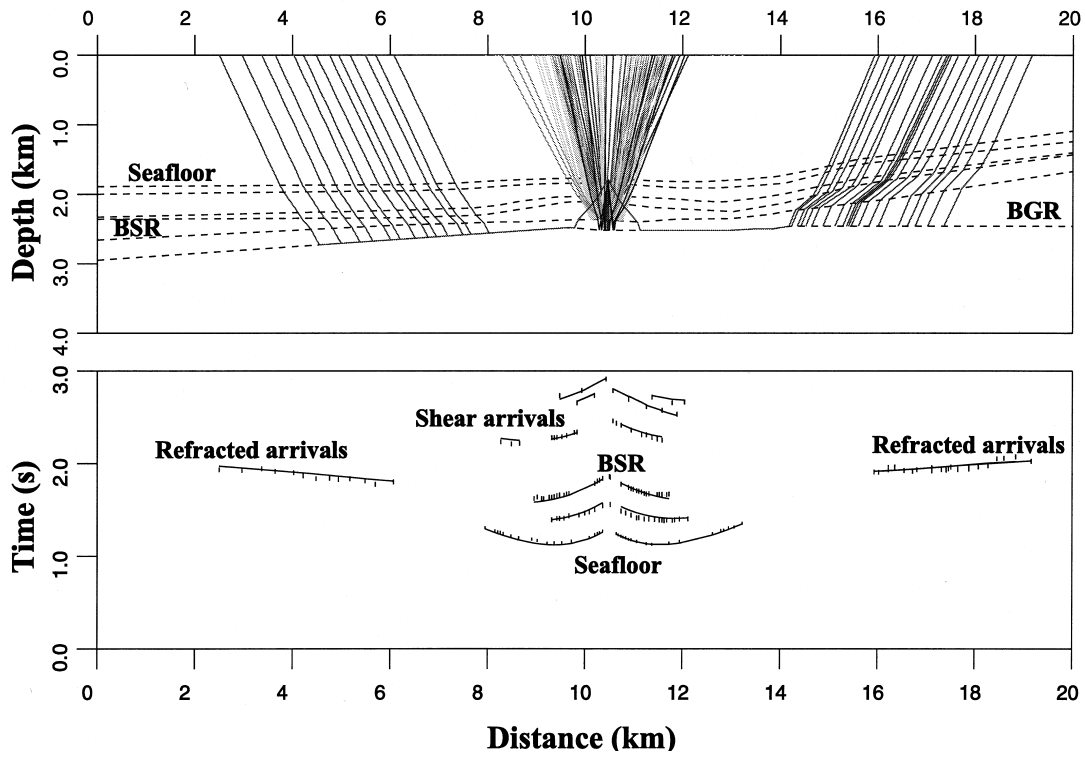

Fig. 4. Top: ray diagram modelled on OBS data. Bottom: comparison of predicted (solid lines) and observed (short vertical lines) travel times. The time is reduced with a velocity of 3 km/s.

velocity to 1.2–1.7 km/s. Below the BGR, we found a velocity of 2.6–2.7 km/s by modelling the refracted waves of the OBS data. Finally, the comparison between the observed and the calculated travel times shows a very good agreement (Fig. 4). We found a normalized χ^2 (Chi-square; e.g. Zelt and Smith, 1992) and a root-mean square (rms) travel time residual equal to 1.225 and 0.025 s, respectively, considering the pick error equal to 0.025 s. In particular, the reflected events at the BSR have a χ^2 of 1.160 and a rms travel time residual of 0.026 s, and the refracted events by the BGR have the χ^2 and rms travel time residual of 1.341 and 0.029 s, respectively.

In order to obtain an estimate of uncertainty for each parameter, we perturbed the related value from that of the final model, hold it fixed, inverted from all the other parameters, and observed the resulting rms travel time residuals (Katzman et al., 1994). We concluded that the average velocity error is equal to about 3%.

3.3. Horizontal components of OBS data

In the horizontal components three strong arrivals at about 2.5, 2.8, and 3 s at minimum offset are evident (Fig. 5). Particle motion plots performed here indicate that the energy is mainly transversal (Fig. 5b–d). For comparison, we also showed the particle motion plot at the BSR (Fig. 5a), where compressional energy is mainly present. We can observe that the horizontal energy increases versus offset and disappears at high incidence angles, as it should be. Note that the minimum horizontal offset is not equal to zero, because the OBS was not in-line with the shot positions. These events can be associated with the converted reflected P wave at the BSR (at 2.5 s at minimum offset), with the converted reflected P wave at the BGR (at 2.8 s at minimum offset), and to the converted transmitted S wave at the BSR and then reflected at the BGR (at 3.0 s at minimum offset), respectively. The inversion of the

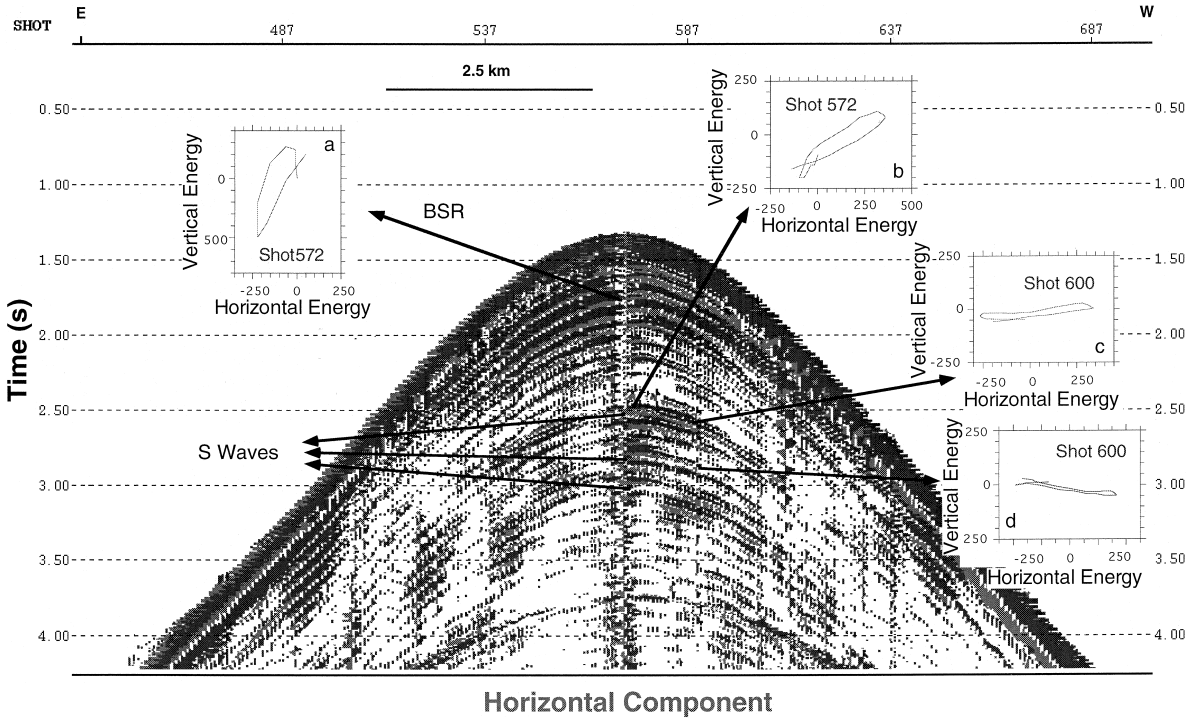

Fig. 5. A horizontal component of OBS data. The inserts indicate the particle motion plot at the BSR (a), at P-converted reflection at the BSR (b and c), and at P-converted reflection at the BGR (d). The converted transmitted S wave at the BSR and then reflected at the BGR (see text) is also shown.

shear wave arrivals allowed us to determine Poisson's ratio of the sediments above the BSR using the Zelt and Smith (1992) method. The inversion revealed, near the OBS position (see dashed lines in Fig. 3), an average Poisson's ratio equal to 0.435 ± 0.005 above the BSR and equal to 0.25 ± 0.02 in the free gas zone (Fig. 3). If we compute the weighted average Poisson's ratio by AVO inversion (see Section 5) above the BSR, we obtain a value of 0.433, that is in good agreement with the value obtained by OBS data inversion. For testing our interpretation of S arrivals, we considered other hypotheses of P-conversion, but all of them gave unacceptable Poisson's ratios.

Regarding the value we obtained in the free gas zone, the laboratory measurements indicated that Poisson's ratio can quickly decrease (Domenico, 1976) versus free gas concentration which is higher than about 8% (Katzman et al., 1994). Our study indicated that free gas in pore spaces is in the order of magnitude of this value. Consequently, we found a free gas concentration where Poisson's ratio is strongly sensitive to small variation of free gas amount. The value of 0.25 is in accordance with the low value of V_p in the layer below the BSR obtained by travel time inversion.

4. Pre-stack depth migration

In order to improve the seismic image, we performed a pre-stack depth migration (the Kirchhoff method) with the obtained velocity field. Fig. 6 shows the section, where bandpass filter (10–75 Hz) and automatic gain control (500 m) were applied. The good result of migration confirms that the velocity structure is reliable (Kim et al., 1996), and underlines the presence of geological structures such as faults and folds in the accreted sediments. In our case, the strongest BSR and the associated low velocity zone below it are coincident with the downslope side of a faulted anticline, and both BSR and BGR cross the stratigraphic structures. The result of migration points

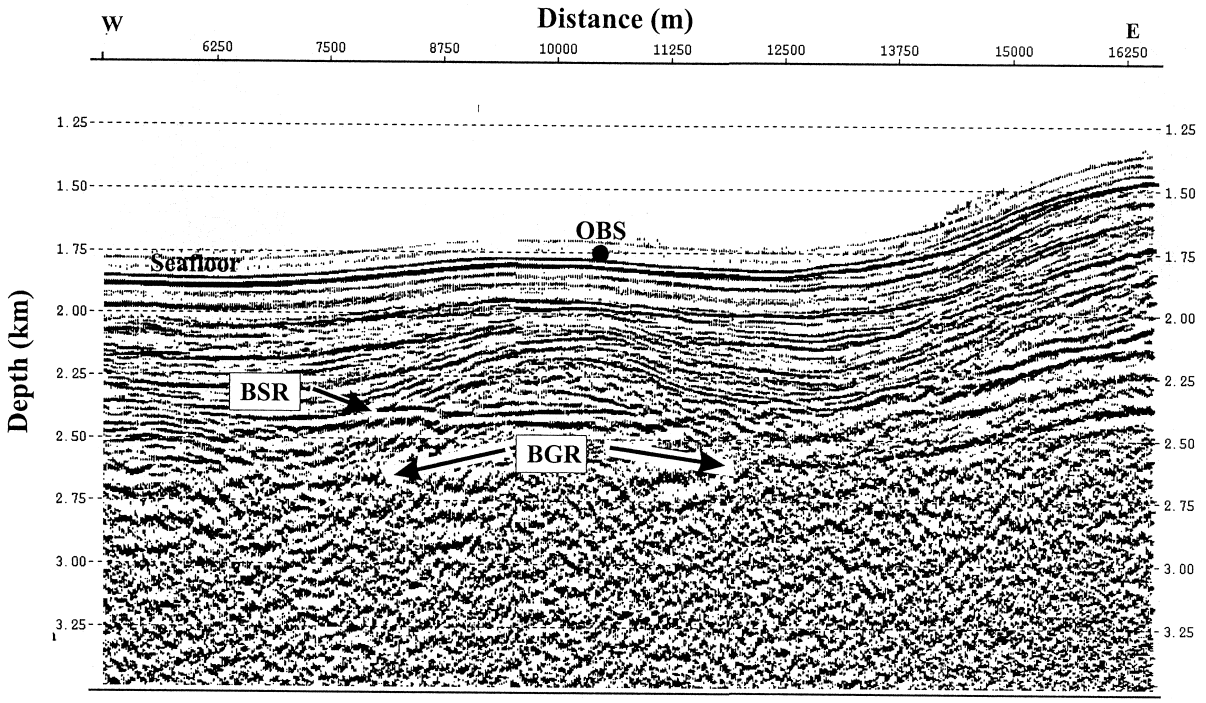

Fig. 6. Pre-stack depth migration of MCS line I97206.

out the BGR, slightly evident in pre-stack and stack section, and displays levels that we interpreted as layer with different concentrations of gas that probably decrease with depth in the free gas zone. In the MCS data, a reflector only, between BGR and the BSR (see Fig. 6), was picked and inverted by tomographic method. This horizon can thus be an internal reflector within the entire gas-bearing layer with a interval velocity lower (MCS data inversion as pointed out) than the velocity obtained below the BSR by refracted events. The gas levels mask the BGR in the reflection data (Jarchow et al., 1994). Hence, the OBS data are indispensable to determine the real base of free gas zone.

5. AVO analysis

An alternative method to determine Poisson's ratio is the AVO analysis of multichannel seismic data from the horizons which have been inverted by the tomographic method. Theoretical analysis (Carcione and Tinivella, 2000) indicates that the increase of free gas saturation causes an increase in the magnitude of the near-offset reflection coefficient. However, for a given gas saturation, it is difficult to evaluate the amount of gas hydrate at low concentration. Fig. 7 represents the reflection coefficients at 25 Hz at the BSR for various concentrations in the pore space of gas hydrate above and free gas below it. In Fig. 7a, the hydrate concentration is fixed at 10%, and in Fig. 7b the free gas saturation is fixed to 10%. More details about the method for evaluating the reflection coefficients and the properties of the sediment and its individual constituents, causing the BSR, are discussed in Carcione and Tinivella (2000). In this case, the AVO anomalies can be of type III and IV according to the classification given by Castagna and Swan (1997). We recall that, for the type III anomalies, the reflection coefficient is negative and its absolute value increases with offset, and for type IV anomalies the coefficient is negative and its absolute value decreases with offset. In Fig. 7, the anomalies are class IV for very high concentrations of gas hydrate, and class III for relatively low concentrations.

In our analysis, we applied the AVO method to

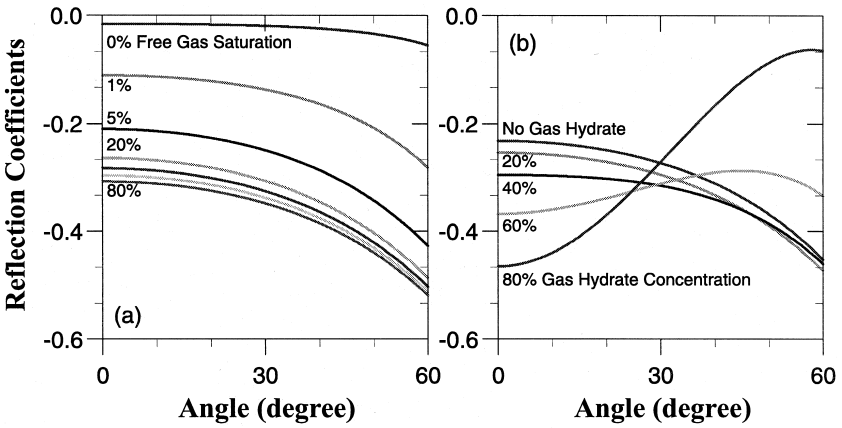

Fig. 7. Theoretical reflection coefficients versus incidence angle, calculated for sediments with 10% gas hydrate concentration (a) and 10% free gas saturation (b).

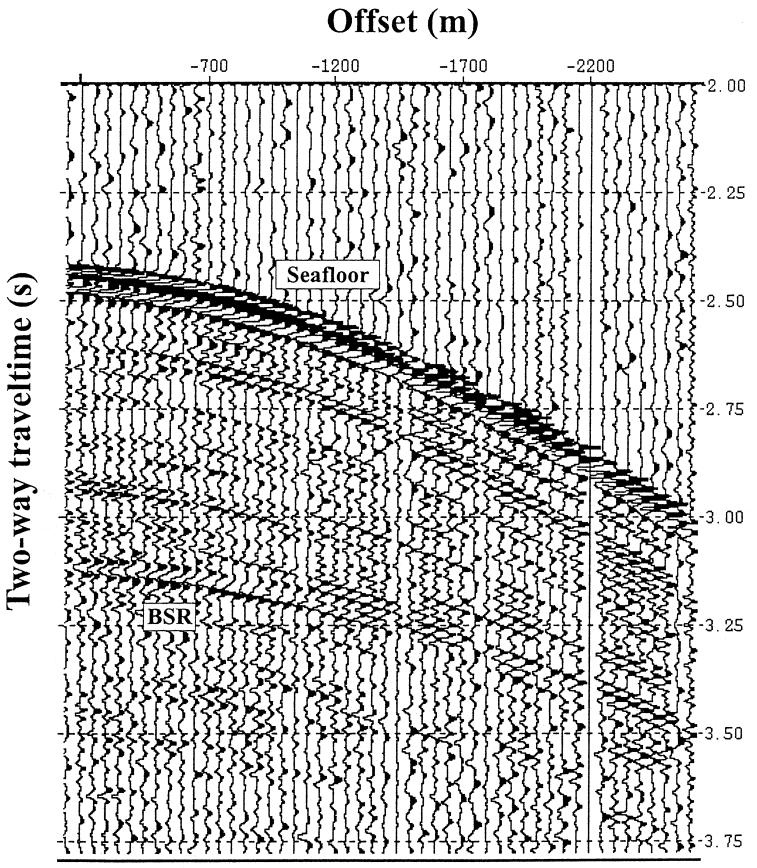

Fig. 8. An example of CDP gathers uncorrected for hydrophone array directivity.

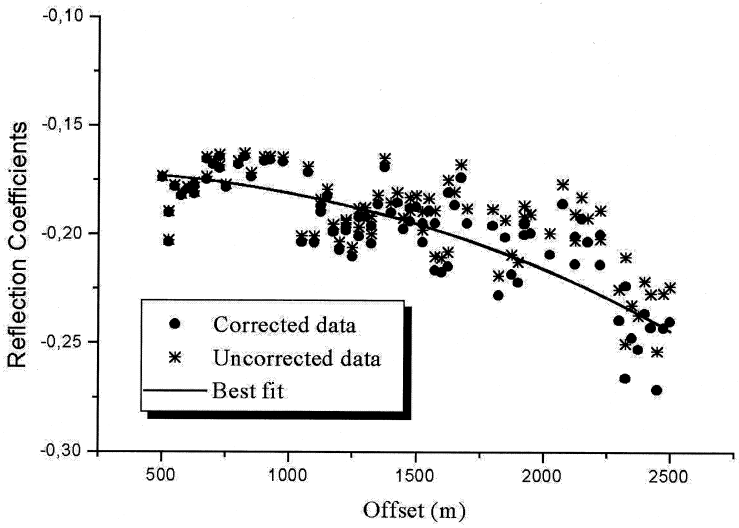

Fig. 9. Reflection coefficients at the BSR extracted from MCS line, uncorrected (stars) and corrected (dots) for hydrophone array directivity. The solid line indicates the theoretical reflection coefficients after minimum search. See Section 5 for details.

selected CDP in three steps: (i) amplitude correction; (ii) calibration of acquisition system; and (iii) AVO inversion. The example of CDP gather (shown in Fig. 8) indicates the general AVO behaviour of the BSR reflection coefficients before hydrophone array directivity correction.

The first step is the amplitude processing whose main purpose is to restore amplitude losses. In order to obtain true-amplitude-offset data, GI gun source and hydrophone receiver attenuation are more important (e.g. Hyndman and Spence, 1992; Ursin and Ekren, 1995). No directivity array correction was applied to the data, because the source (two air guns distributed cross-line) can be treated as a single point source. The hydrophone array is uniform and linear, because the elements are spaced at equal intervals along the seismic line. The hydrophone array attenuation (F) is described by the following formula (Sheriff and Geldart, 1995):

$$F = \left|\sin[\pi n(\Delta x/\lambda)\sin(\theta)]/\{n\sin[\pi(\Delta x/\lambda)\sin(\theta)]\}\right|$$

where n is the number of hydrophones (in our case 32) separated by $\Delta x = 0.806$ m, λ the wavelength, and θ the incidence angle. This correction is important for high offset, as illustrated by Hyndman and Spence (1992) and is shown in Fig. 9 at the BSR in our case.

In the second step, the observed amplitude variations in CDP gathers—we considered the maximum picked amplitude within a window for the reflected event—are scaled for evaluating the reflection coefficients versus offset. The calibration was done by using Warner's approach (Warner, 1990), where the reflection coefficient of the seafloor was evaluated by using the far field signature. The reflection coefficient of the seafloor extracted from the MCS data, is equal to the value determined by the OBS data, i.e. by the ratio between the maximum absolute amplitude of the seafloor multiple and the seafloor primary (Katzman et al., 1994). A spherical divergence correction was applied to the OBS data before this calculation. Another relationship we needed, is the function between the source–receiver offset (x) and the incidence angle (θ); we use the formula suggested by Walden (1991):

$$\sin(\theta) = xV_p/[V_{rms}^2 t(x)]$$

where V_p is the interval velocity of the medium above the interface, V_{rms} the root-mean-square velocity, and $t(x)$ the picked time at x offset. In our AVO analysis, we considered CDP gathers where the structure dips are less than 2°, and no dip corrections are required to determine the incidence angles (Hyndman and Spence, 1992).

The final step relates the experimental coefficients to the physical parameters that caused the reflection:

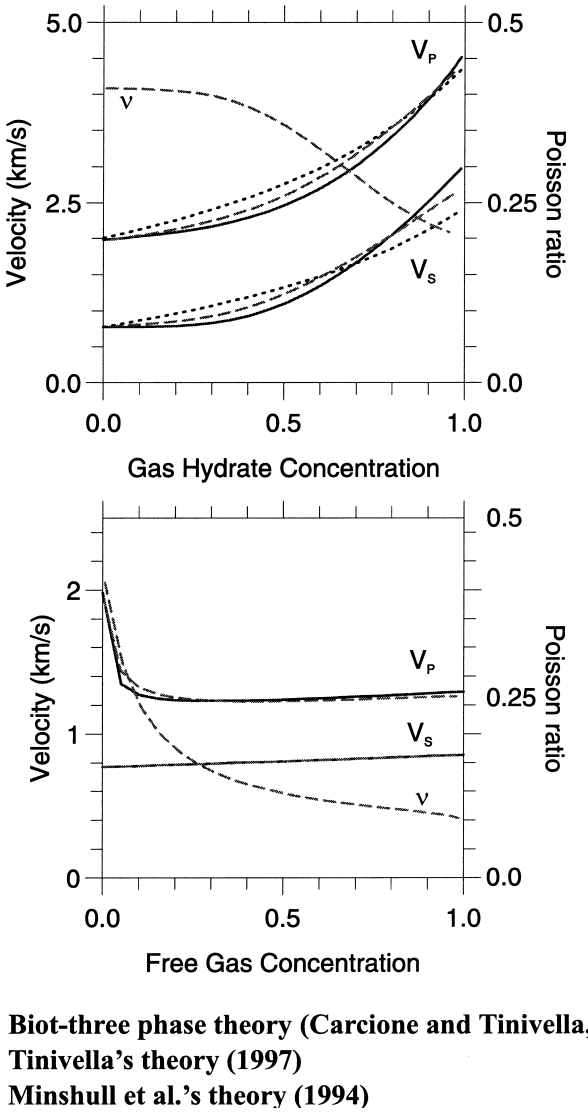

Fig. 10. Compressional and shear wave velocities, and Poisson's ratio (indicated as ν) versus gas hydrate (top) and free gas (bottom) concentration in the pore spaces, according to the type Biot-three phase theory (solid lines; Carcione and Tinivella, 2000), Tinivella's theory (dashed lines; Tinivella, 1999), and Minshull et al.'s theory (dotted lines; Minshull et al., 1994). The parameters to evaluate the curves are in accordance with Minshull et al. (1994).

the V_p and V_s, the density and the quality factors of compressional wave (Q_p) and shear wave (Q_s) for both upper and lower media. The algorithm for determining these parameters is the least-squares method. At a selected reflection, we estimate the physical parameters minimising the function that represents the square difference between the reflection coefficients obtained from seismic data and those obtained from the theory. The theoretical reflection coefficients are obtained for a viscoelastic isotropic media (single-phase model, that includes attenuation effects; e.g. Carcione, 1997). In order to decrease the number of parameters that must be minimised, we fix the parameters of the seawater. The V_p and the density of the

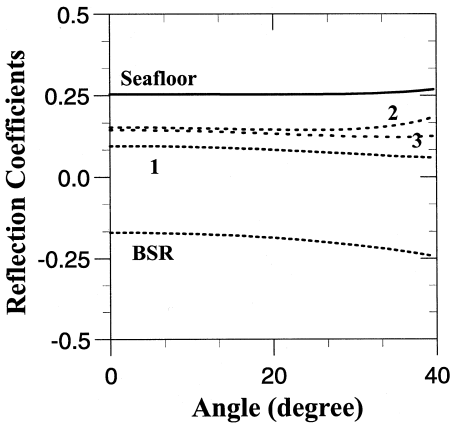

Fig. 11. Theoretical reflection coefficients versus incidence angle that better fit the data at the seafloor, the BSR, and the three horizons (1, 2, and 3) between the two.

seawater are obtained by inversion analysis and empirical relationship between velocity/density, e.g. Fofonoff and Millard (1983), respectively. So, we minimise iteratively only the parameter of the lower layer of each reflection (layer stripping approach). Note that we considered as initial values of the inversion procedure: the V_p obtained by the inversion, the V_s and the densities that are consistent with Hamilton's data set (Hamilton, 1976, 1979). In particular, the densities are less perturbed during the minimisation. The error in assuming that velocity is constant in each layer, is negligible. In fact, the result we obtained minimising the parameters contemporarily of both upper and lower layers is comparable with the result obtained by minimising only the parameters of the lower layer. Q_p and Q_s were assumed to be constant in the sediment and equal to 200 and 100, respectively, according to Pecher et al. (1998). In fact, the lithologic and tectonic characteristics in their studying area are similar to those of the South Shetland margin. The algorithm we use to determine the minimum is the direction set (Powell's) method (Press et al., 1989).

The AVO analysis was applied simultaneously to three selected adjacent CDP gathers, in order to increase the input values for the minimum search. The largest offset traces were rejected because during the acquisition there was very rough sea. The values of Poisson's ratio from the AVO inversions were tested with the OBS data inversion, as discussed in Section 3.2. In the two layers above the BSR, a value of 0.423 and 0.405 are obtained, respectively (Fig. 3). These values indicate that the sediments are not cemented by gas hydrate, as Katzman et al. (1994) pointed out. In fact, cemented sediments—hydrate concentration more than about 50% considering percolation theory; see Section 6—are expected to have high shear wave velocity (Tinivella, 1999). So that Poisson's ratio will decrease slowly when the concentration is low and rapidly when the concentration is high (Fig. 10) with respect to normally consolidated marine sediments (Hamilton, 1979). Katzman et al. (1994) observed that a value of 0.38 is characteristic of strongly hydrated sediments, and for smaller concentration, a value of 0.41 is expected, while the reference value for nonhydrated sediments above and below the BSR is about 0.44 (Hamilton, 1979).

Fig. 9 shows an example of minimum search results: the reflection coefficients at the BSR extracted from the MCS data (stars, uncorrected data; dots, after directivity correction) and the theoretical reflection coefficients (solid line) that fit the data the best. The theoretical reflection coefficients versus incidence angle after AVO analysis at all the selected horizons is shown in Fig. 11. As in the free gas zone thin layers (see Fig. 6) could be present, the analysis requires a more complex AVO study taking into account the layer thickness that we have not included in this work. Therefore, at the BSR, only qualitative information can be extracted from the behaviour of reflection coefficients. In fact, the AVO trend is similar to the case of varying layer thickness for the considered range of incidence angles (Carcione, 1998). We can observe that the trend of reflection coefficients indicates that the amount of gas hydrate is not enough to cement the sediments because an AVO type III anomaly is present (Fig. 11).

6. Estimation of gas hydrate and free gas quantities

The concentration of gas hydrate and free gas in the pore space of marine sediments can be estimated by seismic velocity anomalies applying theoretical models (Tinivella, 1999). The theoretical model we used, is based on Gassmann's equations with an

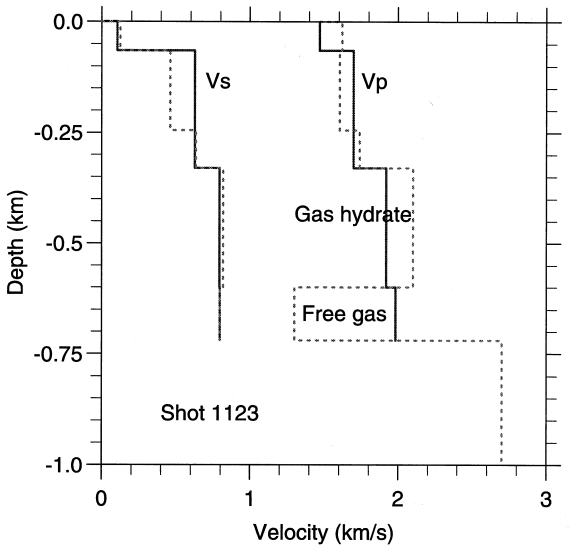

Fig. 12. Comparison between reference velocity curves (without gas hydrate and free gas; solid lines) and seismic velocity profiles after inversion of data (dotted lines). The anomalies can be interpreted as abundance of gas hydrate and free gas in the sediments. The water depth is 1.78 km.

explicit dependence on differential pressure and depth, and it is valid for three different situations: (i) full water saturation; (ii) water and gas hydrate in the pore spaces; and (iii) water and gas in the pore spaces. In order to take into account the effects due to the cementation of grains at high concentrations of gas hydrate, we assume that the rigidity modulus of the solid matrix (μ_{sm}) is affected by cementation of the solid grains by hydrate, using a percolation model (Leclaire, 1992). Percolation theory describes the transition of a system from the continuous state (completely cemented grains) to the discontinuous state (uncemented grains). During this process, connections appear or disappear between the elements of the system. The induced modifications of the system configuration are governed by a general power law so that the shear modulus of the matrix takes the form

$$\mu_{sm} = (\mu_{smKT} - \mu_{sm0})[\phi_h/(1 - \phi_s)]^{3.8} + \mu_{sm0}$$

where μ_{smKT} is Kuster and Toksöz's shear modulus (Kuster and Toksöz, 1974), μ_{sm} is the shear modulus without cementation (no gas hydrate), ϕ_h and ϕ_s are the gas hydrate and solid proportion, respectively. This equation models the increasing stiffness of marine sediments with increasing gas hydrate concentration. The theory indicates an increase of both compressional and shear wave velocities in the presence of gas hydrate, and shows a sudden decrease of V_p and an increase of V_s in presence of the free gas (Fig. 10). To quantify free gas and gas hydrate concentrations, we compared positive V_p and V_s anomalies with reference curves (e.g. normally compacted terrigenous sediments; Hamilton, 1979). The procedure used to estimate the amount of these components was successfully tested against sonic log data and indirect estimation of gas hydrate concentration from chloride content in core logs (Tinivella, 1999).

The parameters used to evaluate the velocities are those given for a normally compacted terrigenous sequence (Hamilton, 1976), that is almost consistent with the velocity profile in the area where the BSR is not present (Tinivella et al., 1998a,b). Poisson's ratio is fixed—we considered the values obtained by AVO inversion above the BSR and the value obtained by OBS data inversion in the free gas zone—and it is used to obtain information about the rigidity of the sediments in each layer. In order to get the amount of clathrates and a preliminary estimation of free gas, we progressively increased the parameters in the theoretical formula related to the concentrations of these components, until we fitted the trend of the seismic velocity curves (V_p and V_s; Fig. 12). The results indicate that the highest gas hydrate concentration near the OBS location is 23% of pore spaces. The theoretical approach gives a free gas amount of 6% of pore space. We underline that the V_p is very sensitive to small amounts of free gas in the sediments, and to free gas distribution in the pore spaces (Domenico, 1977); so, the estimation of free gas from seismic velocity is extremely approximate. This estimation of both gas hydrate and free gas abundance is consistent with the results of Poisson's ratio obtained by the AVO and OBS data inversion in the gas hydrate zone. The uncertainty of estimation of these components depends on the errors of the physical parameters used to evaluate the theoretical velocities. Detailed information derived by well data or more refined analysis of seismic data (e.g. full waveform inversion) could allow more accurate evaluation

of gas hydrate and free gas concentration in pore spaces.

7. Conclusions

Velocity estimations, derived from the joint inversion of reflection and wide-angle travel times, allowed us to identify: (1) the occurrence of positive velocity anomalies associated with the presence of gas hydrates in the sediments; (2) the presence of a low velocity zone, indicating a free gas-bearing sediment layer below the BSR; (3) the effective base of free gas zone; and (4) an estimation of the velocity below it.

The OBS data permitted to evaluate Poisson's ratio near the OBS location, by the inversion of shear wave arrivals in the horizontal components. The compressional velocity resulting from the inversion methods is confirmed by the results of the pre-stack depth migration performed using the obtained velocity structure.

The deviations of velocities from a reference curve indicated that the marine sediments are not cemented by the presence of the clathrates in the pore space, as confirmed by the behaviour of the reflection coefficients obtained from AVO analysis, and from Poisson's ratio estimated by the AVO and OBS data inversion. We can conclude that independent approaches here proposed are valid and can be used to determine useful information about physical properties of marine sediments in areas where no well data are available.

Acknowledgements

We thank Nigel Wardell and Jacque Centonze for assistance in the processing of MCS data. We would like to thank Jose' M. Carcione for useful discussion about AVO inversion. We would like to thank Fabio Cavallini for the preliminary review. We are also grateful to the scientists and the technicians participating in the cruise during data acquisition. In particular, we thank Emanuele Lodolo, Bruno Della Vedova, and Giulio Pellis. Thanks to REDS Group (OGS) for allowing us to use the tomographic inversion software. We appreciate Paul Stoffa and Timothy A. Minshull for careful reviews of the manuscript. The Progetto Nazionale di Ricerche in Antartide (PNRA) supports this work.

References

Andreassen, K., Hart, P.E., MacKay, M., 1997. Amplitude versus offset modelling of the bottom simulating reflection associated with submarine gas hydrate. Marine Geology 137, 25–40.

Barker, P.F., 1982. The Cenozoic history of the Pacific margin of the Antarctic Peninsula: ridge crest–trench interaction. J. Geolog. Soc., London 139, 787–801.

Carcione, J.M., 1997. Reflection and transmission of qP–qS plane waves at a plane boundary between viscoelastic transversally isotropic media. Geophys. J. Int. 129, 669–680.

Carcione, J.M., 1998. AVO effects of a hydrocarbon source-rock layer. E&P Research Center, Norsk Hydro report, Bergen, Submitted for publication.

Carcione, J.M., Tinivella, U., 2000. Bottom simulating reflectors: seismic velocities and AVO effects. Geophysics (in press).

Carrion, P., Boehm, G., Marchetti, A., Pettenati, F., Vesnaver, A., 1993. Reconstruction of lateral gradients from reflection tomography. J. Seismic Exploration 5, 55–67.

Castagna, J.P., Swan, H.W., 1997. Principles of AVO crossplotting. The Leading Edge April.

Domenico, S.N., 1976. Effect of brine-gas mixture on velocity in an unconsolidated sand reservoir. Geophysics 41, 882–894.

Domenico, S.N., 1977. Elastic properties of unconsolidated porous sand reservoirs. Geophysics 42, 1339–1368.

Fofonoff, N.P., Millard Jr, R.C., 1983. UNESCO Technical Papers in Marine Science 44, 15–24.

Hamilton, E.L., 1976. Variations of density and porosity with depth in deep-sea sediments. J. Sediment. Petrol. 46, 280–300.

Hamilton, E.L., 1979. V_p/V_s and Poisson's ratios in marine sediments and rocks. J. Acou. Soc. Am. 66, 1093–1101.

Hyndman, R.D., Spence, G.D., 1992. A seismic study of methane hydrate marine bottom simulating reflectors. J. Geophys. Res. 97, 6683–6698.

Jarchow, C.M., Catchings, R.D., Lutter, W.J., 1994. Large explosive source, wide recording aperture, seismic profiling on the Columbia Plateau, Washington. Geophysics 59, 259–271.

Katzman, R., Holbrook, W.S., Paull, C.K., 1994. Combined vertical-incidence and wide-angle seismic study of a gas hydrate zone, Blake Ridge. J. Geophys. Res. 99, 17 975–17 995.

Kim, Y., Samuelsen, C., Hauge, T., 1996. Efficient velocity model building for prestack depth migration. The Leading Edge 15, 751–753.

Klepeis, K., Lowver, L.A., 1996. Tectonics of the Antarctic-Scotia plate boundary near Elephant and Clarence Islands, West Antarctica. J. Geophys. Res. 101, 20 211–20 231.

Kuster, G.T., Toksöz, M.N., 1974. Velocity and attenuation of seismic waves in two-phase media: Part I. Theoretical formulations. Geophysics 52, 1391–1401.

Later, R., Barker, P., 1991. Effects of ridge crest-trench interaction on Antarctic-Phoenix spreading: forces on a young subdacting plate. J. Geophys. Res. 16, 163–184.

Leclaire, P., 1992. Propagation acoustique dans les milieux poreux soumis au gel—Modelisation et experience. Theese de Doctorat en Physique, Universite Paris 7.

Minshull, T.A., Singh, S.C., Westbrook, G.K., 1994. Seismic velocity structure at a gas hydrate reflector, offshore western Colombia, from full waveform inversion. J. Geophys. Res. 99, 4715–4734.

Pecher, I., Ranero, C.R., von Huene, R., Minshull, T.A., Singh, S.C., 1998. The nature and distribution of bottom simulating reflectors at the Costa Rican convergent margin. Geophys. J. Int. 133, 219–229.

Press, W.H., Flannery, B.P., Teukolsky, S.A., Vatterling, W.T., 1989. Numerical Recipes, Cambridge University Press, New York.

Sheriff, R.E., Geldart, L.P., 1995. Exploration Seismology. Vol. 1: History, Theory, Data Acquisition, Cambridge University Press, New York.

Shipley, T.H., Houston, M.H., Buffler, R.T., et al., 1979. Seismic reflection evidence for widespread occurrence of possible gas-hydrate horizons on continental slopes and rises. AAPG Bull. 63, 2204–2213.

Tinivella, U., 1998. Semi-automatic picking in real seismic data. First Break 16, 47–51.

Tinivella, U., 1999. A method to estimate gas hydrate and free gas concentrations in marine sediments. Bollettino di Geofisica Teorica ed Applicata 40, 19–30.

Tinivella, U., Accaino, F., Lodolo, E., 1998a. Reflected and refracted seismic images of the BSR in the South Shetland Margin (Antarctic Peninsula). Ann. Geophys. 16 (Suppl. 1), C299.

Tinivella, U., Lodolo, E., Camerlenghi, A., Boehm, G., 1998b. Seismic tomography study of a bottom simulating reflector off the South Shetland Margin (Antarctica). In: Henriet, J.-P., Mienert, J. (Eds.). Gas Hydrate, 137. Geological Society, London, pp. 141–151.

Ursin, B., Ekren, O., 1995. Robust AVO analysis. Geophysics 60, 316–326.

Walden, A.T., 1991. Making AVO sections more robust. Geophys. Prospect. 39, 915–942.

Warner, M., 1990. Absolute reflection coefficients from deep seismic reflections. Tectonophysics 173, 15–23.

Zelt, C.A., Smith, R.B., 1992. Seismic traveltime inversion for 2-D crystal velocity structure. Geophys. J. Int. 108, 16–34.